Role of Backbone Charge Rearrangement in the Bond−Dipole and Work Function of Molecular Monolayers

ARTICLE *in* THE JOURNAL OF PHYSICAL CHEMISTRY C · NOVEMBER 2011

Impact Factor: 4.77 · DOI: 10.1021/jp208411f

9 AUTHORS, INCLUDING:

Oded Hod
Tel Aviv University
59 PUBLICATIONS **2,663** CITATIONS
SEE PROFILE

Ron Naaman
Weizmann Institute of Science
304 PUBLICATIONS **5,388** CITATIONS
SEE PROFILE

THE JOURNAL OF PHYSICAL CHEMISTRY C

ARTICLE

pubs.acs.org/JPCC

Role of Backbone Charge Rearrangement in the Bond-Dipole and Work Function of Molecular Monolayers

Tali Aqua,[†] Hagai Cohen,[‡] Ofer Sinai,[§] Veronica Frydman,[‡] Tatyana Bendikov,[‡] Dana Krepel,[∥] Oded Hod,[∥] Leeor Kronik,[§] and Ron Naaman*[,†]

[†]Department of Chemical Physics, [‡]Department of Chemical Research Support, and [§]Department of Materials and Interfaces, Weizmann Institute of Science, Rehovot 76100, Israel

[∥]School of Chemistry, Sackler Faculty of Exact Sciences, Tel Aviv University, Tel Aviv 69978, Israel

Supporting Information

ABSTRACT: Self-assembled organic monolayers serve for modifying the work function of inorganic substrates. We examine the role of the molecular backbone in determining monolayer-adsorbed work function, by considering the adsorption of dithiols with either a partially conjugated or a saturated backbone on the GaAs(001) surface. Using a combination of chemically resolved electrical measurements based on X-ray photoelectron spectroscopy and contact potential difference, together with first principles electronic structure calculations, we are able to distinguish quantitatively between the contributions of the band bending and surface dipole components. We find that the substrates coated by partially conjugated layers possess a larger band-bending, relative to that of the substrates coated by saturated layers. This is associated with an increased density of surface states, likely related to the presence of oxygen. At the same time, the samples coated by partially conjugated layers also possess a larger bond-dipole, with the difference found to result primarily from an extended charge rearrangement on the molecular backbone. The two effects are, in this case, of opposite sign, but a significant net change in work function is still found. Thus, design of the molecular backbone emerges as an additional and important degree of freedom in the design of potential profiles and charge injection barriers in monolayer-based structures and devices.

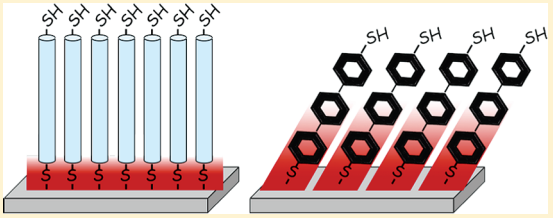

Molecular monolayers adsorbed on metallic or semiconducting surfaces are well-known to affect surface electronic properties and in particular to modify the surface dipole and work function (see, e.g., refs 1−5 for overviews from several perspectives). This effect has already been exploited for a variety of applications, including electronic devices, solar cells, and sensors (see, e.g., refs 6−11). There is therefore ongoing intense interest in understanding, controlling, and utilizing the sensitivity of the surface work function to molecular details.

The most common strategy for molecular modification of surface properties is the use of amphiphilic molecules that self-assemble into organized monolayers. Such molecules typically consist of three parts: A "head" (or "dock") group that binds to the substrate, a "tail" group that is away from the substrate, and a backbone between them. Extensive experimental and theoretical investigations (e.g., refs 3, 4, 12−17) show that for structures possessing a nonpolar backbone, the overall surface dipole, μ, can be largely viewed as a superposition of two leading contributions: $\mu = \mu_{BD} + \mu_{mol}$, where μ_{BD} is a bond-dipole associated with the binding of the docking group to the surface and μ_{mol} is a molecular dipole related to the intrinsic dipole moment determined by the tail group. Choices for the headgroup are typically severely constrained by the need for stable chemical bonding to the substrate. Therefore, tailored modification of the surface work function typically proceeds by rational design of the tail group, e.g., using electron-donating or electron-withdrawing substituents.

The molecular backbone, however, is much more than just a chemically stable spacer between the head and tail groups. The relation between gas phase molecular dipoles and the change induced in the work function is usually given by the Helmholtz equation[2,18]

$$\Delta\phi = \frac{N\mu_g \cos(\theta)}{\varepsilon\varepsilon_0} \quad (1)$$

where μ_g is the gas-phase molecular dipole moment, θ is the tilt angle with respect to the surface normal, N is the surface density of the molecular layer, ε_0 is the relative permittivity of vacuum, and ε is an effective dielectric constant of the layer.[19,20] The actual dipole moment of the adsorbed molecule, μ_{mol}, is (often substantially) smaller than μ_g, due to the effective dielectric constant, which has been shown, both theoretically and experimentally, to depend strongly on the backbone polarizability.[3,14,17,21,22]

Other roles of the backbone are more subtle. The dipole associated with the molecule−substrate bond, μ_{BD}, is largely determined by charge rearrangement upon formation of the substrate-adsorbed molecular monolayer. First principles calculations have shown that, contrary to a naïve picture of chemical bonding, in some cases this rearrangement may be extended and

Received: August 31, 2011
Revised: November 9, 2011
Published: November 14, 2011

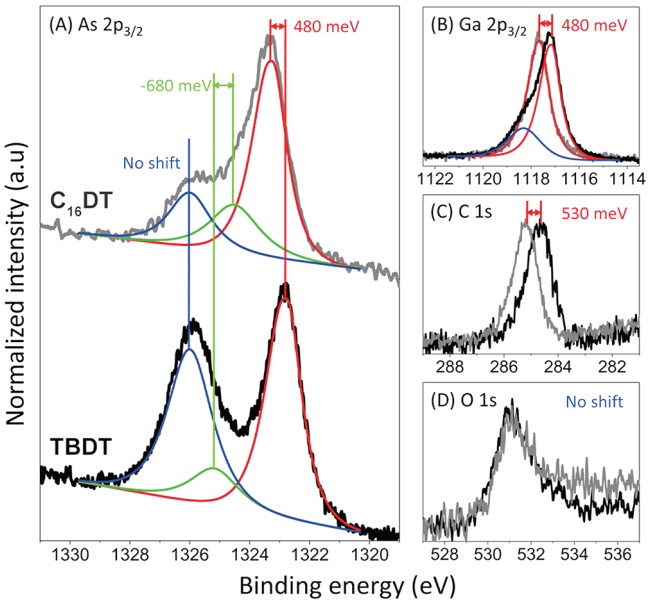

Figure 1. XPS signals corresponding to C_{16}DT-adsorbed (gray lines) and TBDT-adsorbed (black lines) GaAs(001) surfaces. Signals shown are from (A) As $2p_{3/2}$, (B) Ga $2p_{3/2}$, (C) C 1s, and (D) O 1s core levels. Red lines indicate substrate peaks, blue lines indicate substrate oxidized species, and green lines indicate As^S peak.

involve significant charge rearrangement in the backbone as well,[23,24] an observation supported by indirect experimental evidence.[25] Furthermore, in semiconductors the work function is determined not only by the surface dipole, but also by the band bending in the semiconductor. The band bending can also be strongly affected by molecular properties.[18,26]

In this article, we examine the role of the backbone directly, by considering the adsorption of dithiols with either a partially conjugated (TBDT = 4,4′-tribenzenedithiol), or a saturated (C_8DT = 1,8-octanedithiol; and C_{16}DT - 1,16-hexadecanedithiol), backbone on the GaAs(001) surface. Monolayer preparation and characterization is described in detail in the Supporting Information. Owing to symmetry, the gas phase dipole of the dithiols vanishes. Only upon adsorption do different head- and tail-related dipoles emerge, with the difference between them providing a transparent measure for the effects of bonding. Here, we analyze the resulting electronic structure experimentally using chemically resolved electrical measurements (CREM[27]) based on X-ray photoelectron spectroscopy (XPS) and contact potential difference (CPD) measurements. These measurements allow for a clear-cut identification of the various contributions to the work function. Comparison of the experimental results with first principles calculations, based on density functional theory (DFT), reveals the important role that the backbone plays in affecting both the band bending and the surface dipole. In particular, it exposes the importance of extended charge rearrangements in determining the electrical properties of the monolayer-adsorbed substrate.

CREM analysis allows for the study of electrostatic potential variation across the structure based on careful inspection of XPS line positions. In XPS, the kinetic energy of the photoelectron, E_k, is given by

$$E_k = h\nu - E_B - \phi + e\varphi \quad (2)$$

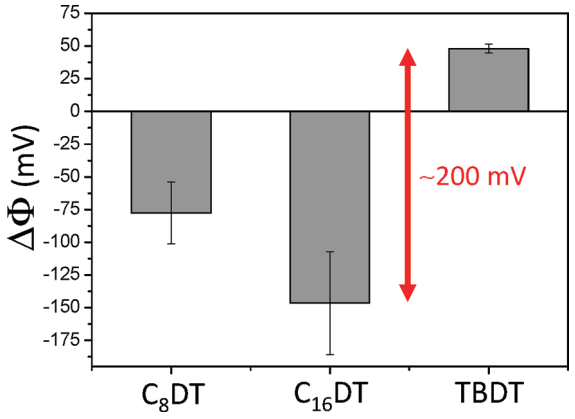

Figure 2. Change in work-function, $\Delta\phi$, upon monolayer adsorption. The zero is taken as the oxidized GaAs substrate.

where $h\nu$ is the photon energy, E_B is the binding energy of the inspected electron state (usually an atomic core level), ϕ is the analyzer work function, e is the electron charge, and φ is the electrostatic potential at the emission site (i.e., at the atom emitting the inspected photoelectron). If the chemical oxidation state, and thus E_B, of a given element is known, one can derive the electrostatic potential at different surface regions, exploiting the various XPS lines as "chemical addresses".

XPS signals corresponding to emission from substrate As $2p_{3/2}$ and Ga $2p_{3/2}$ core levels are shown in Figure 1A,B, respectively, for both the C_{16}DT- and TBDT-coated GaAs substrates. The C_8DT-adsorbed substrate exhibited similar behavior to that of the C_{16}DT-adsorbed one and therefore is not shown. An energy difference of ~500 meV between the C_{16}DT- and TBDT-coated samples, indicated by red lines in the figure, is clearly observed for both core level signals. Because both substrates are grounded, this significant difference in the electrostatic potential at the top surface of the substrate is directly attributed to a ~500 meV difference in surface band bending.

The XPS analysis shows the substrate−molecule interface to consist of oxygen and sulfur atoms (see Supporting Information). Here, we do not find a consistent trend as with the substrate-related peaks. On one hand, the oxide species signals, As^{ox}, Ga^{ox} (blue lines in Figure 1A,B), as well as the O 1s signal (Figure 1D), manifest very minute differences in line positions between the samples. On the other hand, the As^S signal (green line in Figures 1A,B) is shifted significantly to higher energy. We therefore conclude that, for the interface itself, untangling chemical shifts from electrostatic ones is more involved and is not necessary for the current discussion.

Overall differences in the work function among the different samples were deduced from CPD measurements. Changes in the work function of the bare GaAs substrate, upon adsorption of the various monolayers, are given in Figure 2. The work function of the TBDT-adsorbed substrate was found to be ~200 meV higher than that of the C_{16}DT-adsorbed one, but only about ~130 meV higher than that of the C_8DT-adsorbed substrate. The ~70 meV difference between the C_8DT and C_{16}DT is easily rationalized by the fact that a small dipole change corresponding to a work function decrease of ~9 meV per CH_2 unit has been previously found for both layers on gold[28−30] and on GaAs.[31] We note that higher values of per-unit dipole changes were reported for *n*-alkanethiol monolayers on GaAs.[32] However, these changes were attributed to structural

dx.doi.org/10.1021/jp208411f |J. Phys. Chem. C 2011, 115, 24888–24892

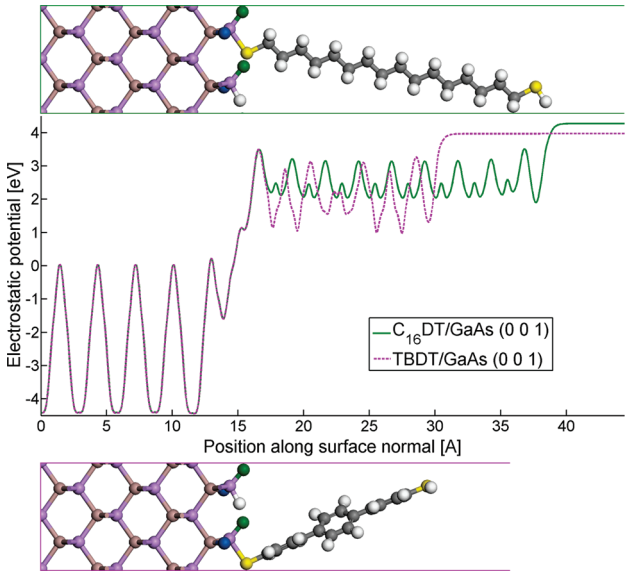

Figure 3. Top and bottom: "ball and stick" model of the C_{16}DT- and TBDT-adsorbed GaAs(001) surface, respectively. Colors indicate the following: brown, Ga; purple, As; gray, C; light gray, H; yellow, S; blue and green, "pseudohydrogen" with $Z = 1.25$ and $Z = 0.5$, respectively. Center: DFT-computed plane-averaged electrostatic potential, relative to the Fermi energy, as a function of distance from the center of the GaAs slab.

modifications and therefore do not contradict the present findings.

The CPD results can also be compared to the XPS C 1s signal, shown in Figure 1C. Here, a shift of 530 meV between the two monolayers is found, of which 300 meV is attributed to chemical shifts, namely, to the different chemical states of conjugated and saturated hydrocarbon.[33] The remaining ~230 meV difference is roughly consistent with the CPD data. Note that the effective depth probed by the integral C 1s line exceeds the top atoms and there is contribution from middle chain carbons. The XPS S 2p signal of the top sulfur atom yields as well a ~170 meV electrostatic difference between the surfaces with the TBDT and C_{16}DT monolayers, in rough agreement with the values above.

In order to further interpret our findings, we performed first principles electronic structure calculations for C_{16}DT and TBDT adsorbed on GaAs(001), using density functional theory (DFT). The molecule-adsorbed surfaces were modeled with a periodic slab approach, and all calculations were performed using the Perdew–Burke–Ernzerhof (PBE) generalized-gradient approximation functional,[34] using a planewave basis set while treating the core electrons using the projector augmented wave method, as implemented in the VASP code.[35] A $9 \times 9 \times 1$ Monkhorst–Pack[36] *k*-point sampling scheme and default planewave cutoff parameters were used throughout. We note that the PBE functional typically encounters difficulties in the presence of strongly localized states due to self-interaction errors.[37] However, for the simple aromatic and aliphatic systems of the type studied here it has been repeatedly shown that adsorbate-induced work function changes due to dipolar effects are captured accurately by PBE calculations, not just qualitatively but even quantitatively.[38−40]

As shown in Figure 3, the adsorbed molecules were assumed to bind to the As atoms with a 50% coverage, i.e., one adsorbate molecule in each 2×2 surface cell. Passivation of the GaAs(001) surface was achieved with the aid of pseudohydrogen atoms,[41]

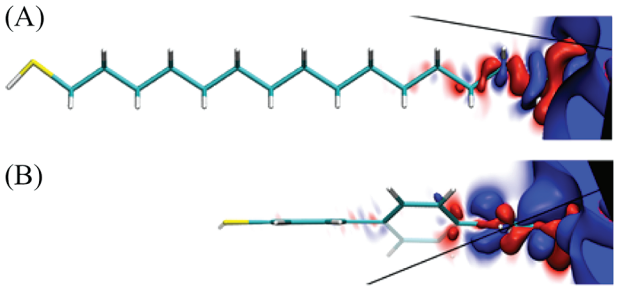

Figure 4. Charge transfer in (A) C_{16}DT and (B) TBDT upon adsorption on the GaAs(001) surface (right). Blue and red represent regions where the electronic charge density is increased or decreased, respectively. Three dimensional iso-surfaces are drawn at an absolute value of 0.25 me/Å^3. The black lines represent the surface normal.

namely fictitious atoms with fractional charges that mimic the polarity of the broken bonds. Obviously this oxygen-lacking, fractional-charge-atom containing surface is not meant to be a fully realistic model for the adsorbed GaAs surface. However, as we show below, it is sufficient for capturing the salient differences between the two adsorbed molecules. Following geometry optimization, based on an asymmetric slab consisting of 14 atomic GaAs layers, the slab was "doubled" so as to create a symmetric slab consisting of 19 atomic GaAs layers, with 12 Å of vacuum above the molecular layer. The plane-averaged electrostatic potential, also shown in Figure 3, was then computed for the symmetrized cell, so as to avoid spurious dipolar terms present in the asymmetric slab.[42] Convergence of both geometry and electrostatic potential with respect to the amount of vacuum was verified explicitly.

Simulations of the type performed here inherently exclude the surface band bending because the simulation slab is thin and undoped. They do, however, allow for determining dipole-related changes in the work function, because the latter is computed as the difference between the electrostatic potential at vacuum and the Fermi energy.[43] The computed work function for the C_{16}DT- and TBDT-adsorbed slabs yields a ~300 meV higher work function for the alkylated surface. This is consistent with the experimental results once the ~500 meV higher band bending with TBDT is deduced from the ~200 meV higher overall work function with TBDT. The quantitative agreement should not be overinterpreted. Because the surface atomic structure is not identical to the experimental one, the achievement of complete quantitative agreement is clearly fortuitous. However, the qualitative agreement is satisfying and allows for further interpretation of the experimental results by means of analysis of the theoretical ones.

The oscillations seen in the electrostatic potential curves of Figure 3 occur because the plane-averaged potential plotted there is microscopic. It includes all contributions of nuclei and electrons and *cannot* be directly compared to the mean electrostatic potential at atomic sites, used in the CREM analysis. Specifically, this potential can be meaningfully related to an effective surface dipole only at extremal values, which correspond to planes that divide the structure into neutral subunits, such that partial dipoles are well-defined.[42] Using these extrema as a guideline, Figure 3 shows that the potentials in both structures are virtually identical at the extremum corresponding to the surface-side S–C bond. The main part of the potential difference between the two adsorbates occurs along the backbone, with negligible variation

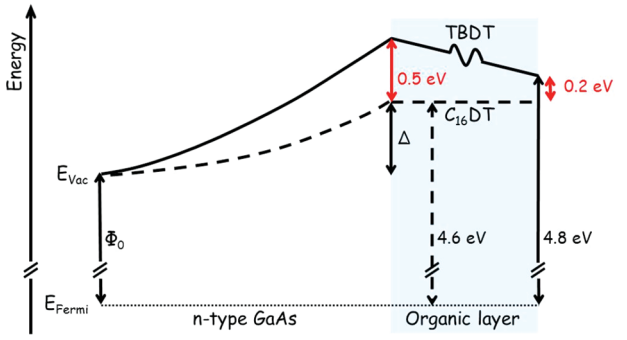

Figure 5. Gross change in local vacuum level as a function of position along the surface normal, shown from the bulk toward the adsorbed monolayer (not to scale), with detailed potential variation shown in Figure 3. The solid line corresponds to the sample coated with the TBDT and the dashed line to the sample with the C_{16}DT monolayer. The potential across the monolayer is shown schematically.

along the C_{16}DT backbone, but a significant drop along the TBDT backbone, primarily along the phenyl ring closest to the substrate.

To understand this potential drop, adsorption-induced charge rearrangement in the molecules was analyzed by computing the difference in charge distribution between the adsorbed molecule and the free molecule in the same geometry, with the As atom bound to the S atom in the headgroup replaced by H and allowed to relax. The results of this analysis are shown in Figure 4. Clearly, the response of the TBDT molecule to the surface extends significantly further into the backbone than that of the C_{16}DT. This is reasonable, given the larger polarizability of TBDT. The significant charge reorganization in the vicinity of the phenyl ring closest to the surface matches the above observations on the electrostatic potential drop and suggests that it is this reorganization of charge that causes lowering of the work function along the backbone of the TBDT.

Importantly, Figure 3 also rules out two alternative mechanisms that *a priori* could have explained the observed work function trends. First, the electrostatic potential difference between the two layers at the center of the outer S−C bond is already ∼230 meV out of the total ∼300 meV. This indicates that difference in the S−C dipole at the tail group, due to the difference between the conjugated and saturated environments, does not dominate the overall difference in work function between the two systems. Second, the two monolayers also differ in their molecular tilt angle. Experimentally, on the basis of ellipsometry and the XPS data, they are found to be 0° and 35° from the surface normal for the C_{16}DT and TBDT, respectively. Computationally, they are found to be 9.6° and 22.2°. The ∼10−15° difference between theory and experiment is partly due to the surface model chosen and partly due to the nearly absent description of dispersive interactions in the PBE functional.[44] While generally a different backbone-dictated tilt can be very important for monolayer electrostatics,[23] note that here the experimental uncertainty in the angle is itself ∼10° and that in any case the significant qualitative difference in electrostatic potential cannot be dominated by the difference in tilt angle. It is a result of qualitative differences in the electronic structure.

The different monolayers affect the work function differently owing to changes in both band bending and surface dipole, as summarized in Figure 5. While absolute values of band bending have not been measured, the XPS analysis shows that the TBDT increases the band bending, and ergo the work function, by ∼500 meV with respect to C_{16}DT. Likely, this is due to increased oxidation with TBDT, which results in more surface states. As for the surface dipole, both XPS and CPD data indicate that here TBDT lowers the work function by ∼200 meV with respect to C_{16}DT. DFT-based analysis reveals that this change is primarily due to the much larger response of the molecular backbone for TBDT, which results in the evolution of a significant dipole on it. The two effects cancel each other only partially, resulting in a net difference of ∼200 meV. Further comparison to C_8DT shows that these conclusions are largely independent of the chain length, save for a small additional dipolar contribution.

In conclusion, we examined the role of the molecular backbone in determining monolayer-adsorbed work function by considering the adsorption of dithiols with either a partially conjugated or a saturated backbone on the GaAs(001) surface. Using a combination of XPS-based CREM analysis and CPD measurements, together with DFT-based first principles calculations, we were able to distinguish quantitatively between the different contributions of the band bending and surface dipole components. While the former has to do with monopolar surface charge contributions, the latter is affected by molecular dipoles. In the dithiols studied here, the gas phase dipole vanishes by symmetry, but upon adsorption head- and tail-related dipoles emerge, with the difference between them providing a transparent measure for the effects of extended charge rearrangement on the observed changes. Thus, design of the molecular backbone emerges as an additional degree of freedom in the design of monolayer-based structure and devices.

■ ASSOCIATED CONTENT

Supporting Information. Details on the monolayer preparation and characterization. This material is available free of charge via the Internet at http://pubs.acs.org.

■ ACKNOWLEDGMENT

R.N. acknowledges the partial support by the US-DOE (Grant ER46430). L.K. acknowledges the partial support of the Lise Meitner Minerva Center for Computational Chemistry. L.K. and R.N. acknowledge the support of the Israel Science Foundation through its Centre of Excellence Program. O.H. acknowledges the partial support of the Center for Nanoscience and Nanotechnology at Tel Aviv University and the Lise-Meitner Minerva Center for Computational Quantum Chemistry.

■ REFERENCES

(1) Ishii, H.; Sugiyama, K.; Ito, E.; Seki, K. *Adv. Mater.* **1999**, *11*, 605–625.
(2) Ashkenasy, G.; Cahen, D.; Cohen, R.; Shanzer, A.; Vilan, A. *Acc. Chem. Res.* **2002**, *35*, 121–128.
(3) Natan, A.; Kronik, L.; Haick, H; Tung, R. *Adv. Mater.* **2007**, *19*, 4103–4117.
(4) Heimel, G.; Romaner, L.; Zojer, E.; Bredas, J. *Acc. Chem. Res.* **2008**, *41*, 721–729.
(5) De Renzi, V. *Surf. Sci.* **2009**, *603*, 1518–1525.
(6) Naaman, R. *Phys. Chem. Chem. Phys.* **2011**, *13*, 13153–13161.
(7) Cahen, D.; Naaman, R.; Vager, Z. *Adv. Funct. Mater.* **2005**, *15*, 1571–1578.
(8) Vilan, A.; Yaffe, O.; Biller, A.; Salomon, A.; Kahn, A.; Cahen, D. *Adv. Mater.* **2010**, *22*, 140–159.

(9) Arya, S. K.; Solankia, P. R.; Datta, M.; Malhotra, B. D. *Biosens. Bioelectron.* **2009**, *24*, 2810–2817.
(10) Sessolo, M.; Bolink, H. J. *Adv. Mater.* **2011**, *23*, 1829–1845.
(11) Hsu, J. W. P.; Lloyd, M. T. *MRS Bull.* **2010**, *35*, 422–428.
(12) Adam, N. K.; Danielli, J. F.; Harding, J. B. *Proc. R. Soc. London, Ser. A* **1934**, *147*, 491–499.
(13) Taylor, D. M.; Bayes, G. F. *Phys. Rev. E* **1994**, *49*, 1439–1449.
(14) Natan, A.; Zidon, Y.; Shapira, Y.; Kronik, L. *Phys. Rev. B* **2006**, *73*, 193310:1–4.
(15) Rusu, P.; Brocks, G. *J. Phys. Chem. B* **2006**, *110*, 22628–22634.
(16) Sushko, M. L.; Shluger, A. L. *Adv. Funct. Mater.* **2008**, *18*, 2228–2236.
(17) Heimel, G.; Rissner, F.; Zojer, E. *Adv. Mater.* **2010**, *22*, 2494–2513.
(18) Kronik, L.; Shapira, Y. *Surf. Sci. Rep.* **1999**, *37*, 1−206, section 5.2.
(19) Romaner, L.; Heimel, G.; Ambrosch-Draxl, C.; Zojer, E. *Adv. Funct. Mater.* **2008**, *18*, 3999–4006.
(20) Natan, A.; Kuritz, N.; Kronik, L. *Adv. Funct. Mater.* **2010**, *20*, 2077–2084.
(21) Fukagawa, H.; Yamane, H.; Kera, S.; Okudaira, K. K.; Ueno, N. *Phys. Rev. B* **2006**, *73*, 245310:1–5.
(22) Peor, N.; Sfez, R.; Yitzchaik, S. *J. Am. Chem. Soc.* **2008**, *130*, 4158–4165.
(23) Wang, L. J.; Rangger, G. M.; Romaner, L.; Heimel, G.; Bučko, T.; Ma, Z. Y; Li, Q. K.; Shuai, Z.; Zojer, E. *Adv. Funct. Mater.* **2009**, *19*, 3766–3775.
(24) Ma, Z. Y; Rissner, F.; Wang, L. J.; Heimel, G.; Li, Q.; Shuai, Z.; Zojer, E. *Phys. Chem. Chem. Phys.* **2011**, *13*, 9747–9760.
(25) Ray, S. G.; Cohen, H.; Naaman, R.; Liu, H.; Waldeck, D. H. *J. Phys. Chem. B* **2005**, *109*, 14064–14073.
(26) (a) Cohen, R.; Kronik, L.; Shanzer, A; Cahen, D.; Liu, A.; Rosenwaks, Y.; Lorenz, J.; Ellis, A. B. *J. Am. Chem. Soc.* **1999**, *121*, 10545–10553. (b) Cohen, R.; Kronik, L.; Vilan, A.; Shanzer, A.; Rosenwaks, Y.; Cahen, D. *Adv. Mater.* **2000**, *12*, 33–37.
(27) Cohen, H. *Appl. Phys. Lett.* **2004**, *85*, 1271–3.
(28) Ichii, T.; Fukuma, T.; Kobayashi, K.; Yamada, H.; Matsushige, K. *Nanotechnology* **2004**, *15*, S30–S33.
(29) Lu, J.; Delamarche, E.; Eng, L.; Bennewitz, R.; Meyer, E.; Guntherodt, J. H. *Langmuir* **1999**, *15*, 8184–8188.
(30) Evans, S. D.; Ulman, A. *Chem. Phys. Lett.* **1990**, *170*, 462–466.
(31) Capua, E. Ph.D. Thesis, Weizmann Institute, 2009.
(32) Marshall, G. M.; Lopinski, G. P.; Bensebaa, F.; Dubowski, J. J. *Langmuir* **2009**, *25*, 13561–13568.
(33) Beamson, G.; Briggs, D. *High Resolution XPS of Organic Polymers; The Scienta ESCA300 Database*; John Wiley & Sons: Chichester, U.K, 1992.
(34) Perdew, J. P.; Burke, K.; Ernzerhof, M. *Phys. Rev. Lett.* **1996**, *77*, 3865–3868.
(35) Kresse, G.; Furthmüller, J. *Comput. Mater. Sci.* **1996**, *6*, 15–50.
(36) Monkhorst, H. J.; Pack, J. D. *Phys. Rev. B* **1976**, *13*, 5188–5192.
(37) Kümmel, S.; Kronik, L. *Rev. Mod. Phys.* **2008**, *80*, 3–60.
(38) Fatemi, V.; Kamenetska, M.; Neaton, J. B.; Venkataraman, L. *Nano Lett.* **2011**, *11*, 1988–1992.
(39) Track, A. M.; Rissner, F.; Heimel, G.; Romaner, L.; Käfer, D.; Bashir, A.; Rangger, G. M.; Hofmann, O. T.; Bučko, T.; Witte, G.; Zojer, E. *J. Phys. Chem. C* **2010**, *114*, 2677–2684.
(40) Magid, I.; Burstein, L.; Seitz, O.; Segev, L.; Kronik, L.; Rosenwaks, Y. *J. Phys. Chem. C* **2008**, *112*, 7145–7150.
(41) Huang, X.; Lindgren, E.; Chelikowsky, J. R. *Phys. Rev. B* **2005**, *71*, 165328:1–6.
(42) Natan, A.; Kronik, L.; Shapira, Y. *Appl. Surf. Sci.* **2006**, *252*, 7608–7613.
(43) Fall, C. J.; Binggeli, N.; Baldereschi, A. *J. Phys.: Condens. Matter* **1999**, *11*, 2689–2696.
(44) Riley, K. E.; Pitonák, M.; Jurecka, P.; Hobza, P. *Chem. Rev.* **2010**, *110*, 5023–63.